16-channel hybrid WDM-PDM-MDM (de) multiplexer for multi-band large-capacity optical transmission system based on thick Si_3N_4 platform

Deyue Ma†, Xiwen He†, Chen Zhou, Mingyue Xiao, Jiqiao Liu, Weibiao Chen*, and Zhiping Zhou*

Abstract—We propose a novel design of hybrid multi-band wavelength/polarization/mode (de)multiplexer based on 800 nm thick Si_3N_4 platform. The 16 channels are enabled by asymmetric rib polarization beam splitters, subwavelength polarization rotators and asymmetric directional couplers, consisting of two operating frequency bands, dual polarization and four transmission modes (2×2×4). A broad bandwidth range from 930 nm to 1600 nm is supported simultaneously on a same chip. This chip can achieve low insertion loss and crosstalk in the 100 nm range near the center wavelength (1550 nm and 980 nm). Our results demonstrate that all channels of the (de)multiplexer have an average insertion loss of less than 1.1 dB. In addition, the crosstalk in the same band is less than -20 dB, while less than -15 dB in different frequency bands. This hybrid (de)multiplexer chip has a great potential for application in multi-band large-capacity optical communication systems, especially in integrated multi-band multiplexing systems.

Index Terms—multi-band, multiplexing ,hybird (de)MUX, WDM, PDM, MDM

I. Introduction

WITH the rapid development in communication, sensing, artificial intelligence, and other fields, current optical transmission systems are struggling to meet the rising capacity demands. With the extended spectrum, the Multi-band (MB) optical networks have great potential to meet the requirement. Integrating wavelength-division-multiplexing (WDM) technology, MB network can achieve large number of channels in-parallel [1]–[5]. However, the cost increases significantly with too many wavelength channels involved [6]. Therefore, it is not an sufficient solution for addressing transmission capacity bottlenecks.

As an alternative, Hybrid (de)multiplexing technology can present a direct and highly efficient approach for expanding the number of transmission channels by integrating WDM with mode-division-multiplexing (MDM) and polarization-division-multiplexing (PDM) techniques [7]–[10]. Implementing hybrid (de)multiplexing technology in the MB transmission system represents a pioneering approach to overcoming capacity limitation, enabling the maximization of optical communication system volume. Furthermore, the MB hybrid (de)multiplexing system, which supports the 980 nm band, serves not only as an optical interconnection tool but also as a pump source for on-chip amplifiers, enhancing transmission distance, and signal quality [11]–[14].

The core component facilitating MB hybrid (de)multiplexing is the (de)multiplexer ((de)MUX). Many excellent work has been reported into on-chip (de)MUX technology, including systems with multiple transmission channels utilizing WDM [15]–[17], interconnection chips incorporating MDM technology [18]–[23], (de)MUXs designed for mode-polarization hybrid (de)multiplexing [24]–[26], (de)MUXs combining WDM and MDM techniques [27]–[29], on-chip multi-channel hybrid (de)MUXs enabling simultaneous wavelength-/polarization-division-multiplexing [30]–[32], and multidimensional (de)multiplexing systems integrating WDM, PDM, and MDM [31], [33]. However, the majority of these studies focus on individual band, with rare research on on-chip MB (de)MUXs, especially hybrid (de)MUX.

In this work, we introduce a technique for designing a wideband MB hybrid (de)multiplexer incorporating WDM, PDM, and MDM. Integrating subwavelength grating polarization rotator (SWGPR) and asymmetric rib polarization beam splitter (ARPBS) in the design enables the (de)MUX to support a wide operational bandwidth of 100 nm centered at both 980 nm and 1550 nm on a single chip,

This work was supported by the Key Program of the National Natural Science Foundation of China under Grant 62035001 (Corresponding: Zhiping Zhou.),the Shanghai Science and Technology Innovation Action Plan under grant number 22dz208700,the International Partnership Program of Chinese Academy of Sciences under grant number 18123KYSB20210013.

Deyue Ma, Xiwen He, Jiqiao Liu and Weibiao Chen are with the Aerospace Laser Technology and Systems Department,Shanghai Institute of Optics and Fine Mechanics,Chinese Academy of Sciences, Shanghai 201800, China(e-mail:madeyue@siom.ac.cn;hexiwen@siom.ac.cn;liujiqiao@siom.ac.cn; wbchen@siom.ac.cn).

Deyue Ma, Xiwen He, Jiqiao Liu and Weibiao Chen are with the Center of Materials Science and Optoelectronics Engineering, University of Chinese Academy of Sciences, Beijing 100049, China.

Zhiping Zhou is with the State Key Laboratory of Advanced Optical Communications Systems and Networks, School of Electronics, Peking University, Beijing 100871, China(e-mail:zjzhou@pku.edu.cn).

Chen Zhou is with the School of Physical Sciences, University of Science and Technology of China, Hefei 230026, China(e-mail:zhouchen@siom.ac.cn).

Mingyue Xiao is with the School of Microelectronics, Shanghai University, Shanghai 201800, China(e-mail:xiaomingyue@siom.ac.cn).

First Author and Second Author contribute equally to this work.

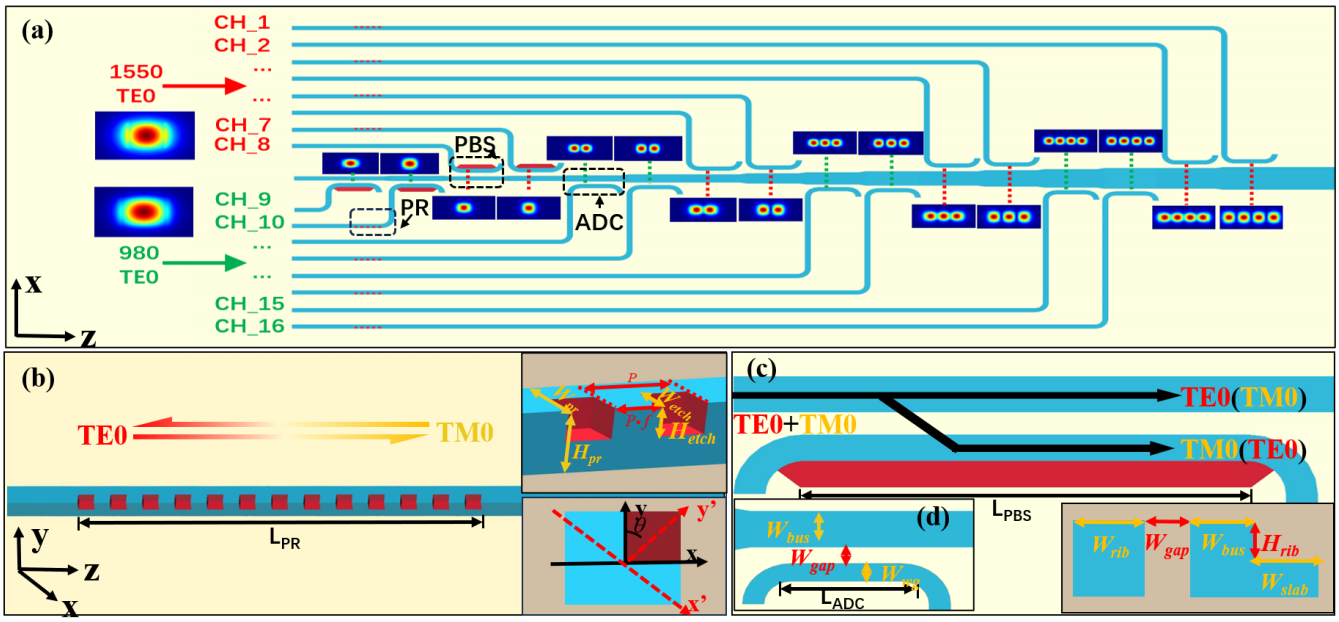

Fig. 1. The schematic configuration of the designed Si_3N_4 MB hybrid WDM-PDM-MDM (de) multiplexer;(b) Structure fo the subwavelength gating polarization rotator (SWGPR) (the insets show the SWG with key parameters and optical axis deflection Angle θ); (c)The structure and key parameters of the asymmetric rib polarization beam splitter (ARPBS);(d) The structure and key parameters of the asymmetric directional coupler (ADC).

allowing for a wavelength range spanning from 930 nm to 1600 nm while maintaining low loss and crosstalk. With a wide operational bandwidth and numerous channels, the (de)multiplexer paves the way for high-capacity optical network communication. Additionally, our work also finds extensive application in other MB systems, including on-chip amplification and detection systems.

II. Theory and Design

In this work, a MB hybrid 980 nm/ 1550 nm (de)MUX is designed on 800 nm thick Si_3N_4 platform, shown in Fig.1(a). The thick Si_3N_4 platform, in comparison to the SOI platform, provides a wider transparent window spanning from visible light to mid-infrared light. It also exhibits lower nonlinear effect and lower loss. Additionally, this platform features a narrower refractive index gap between Si_3N_4 and the SiO_2 substrate, contributing to the enhancement of transmission mode stability [34], [29], [35]. The (de)MUX comprises SWGPRs,ARPBSs and asymmetric directional couplers (ADCs) as depicted in Fig. 1. This (de)MUX accommodates 16 channels (2×2×4), including two operational bands at 1550 nm and 980 nm, two polarization states: Transverse Electric (TE) and Transverse Magnetic (TM), and four modes ($TE(M)_0, TE(M)_1, TE(M)_2, TE(M)_3$).

A. Subwavelength grating polarization rotator

The polarization rotator (PR) is implemented on the (de)MUX for enhancing the conversion between the TE_0 mode and the modes in the TM state. Enhanced birefringence effect is realized with the employment of the subwavelength grating (SWG) [36]. This structure offers board operation bandwidth due to its characteristic of wavelength insensitivity. Additionally, low transmission loss of subwavelenth structure has been demonstrated [37]. The SWGPR is shown in Fig. 1 (b).

For the light incident vertically on the SWG waveguide, the grating structure can be regarded as a uniform medium whose refractive index is between the waveguide medium and the substrate medium. The equivalent refractive index satisfies the following relationship [38], [39]:

$$\begin{pmatrix} n_{xx} & & \\ & n_{yy} & \\ & & n_{zz} \end{pmatrix} = \begin{pmatrix} n_o & & \\ & n_e & \\ & & n_o \end{pmatrix} \tag{1}$$

$$n_o^2 = f n_{Si3N4}^2 + (1-f)\, n_{SiO2}^2 \tag{2}$$

$$\frac{1}{n^2} = \frac{f}{n_{Si3N4}^2} + \frac{1-f}{n_{SiO2}^2} \tag{3}$$

Where n_{xx}, n_{yy}, n_{yy} and are the refractive indices along the x, y, and z axes; f are the subwavelength grating duty cycle; n_{SiO_2} and $n_{Si_3N_4}$ are the refractive indices of SiO2 and Si3N4, respectively.

The equivalent refractive index distribution of cross section is asymmetric for partially etching the straight waveguide into SWG. And this structure deflects the optical axis in the waveguide. The deflection angle between the optical axis and the fixed coordinate system in the waveguide structure is defined as θ (where the fixed coordinate system is defined as the Cartesian coordinate system, with the X-axis parallel to the waveguide epitaxial

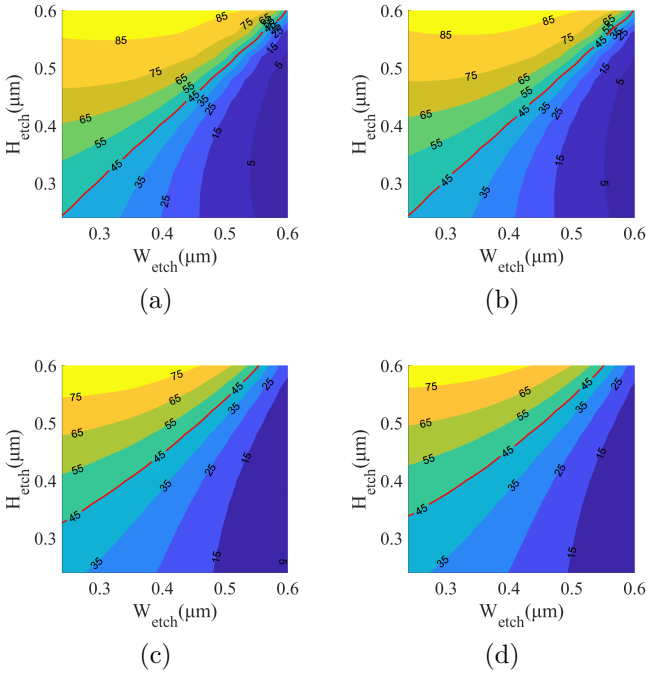

Fig. 2. The calculated optical axis deflection angle θ with varied H_{etch} ,W_{etch} and duty f. (a)(b) 980 nm ((a)f = 0.3;(a)f = 0.4);(c)(d) 1550 nm ((c)f = 0.3;(d)f = 0.4).

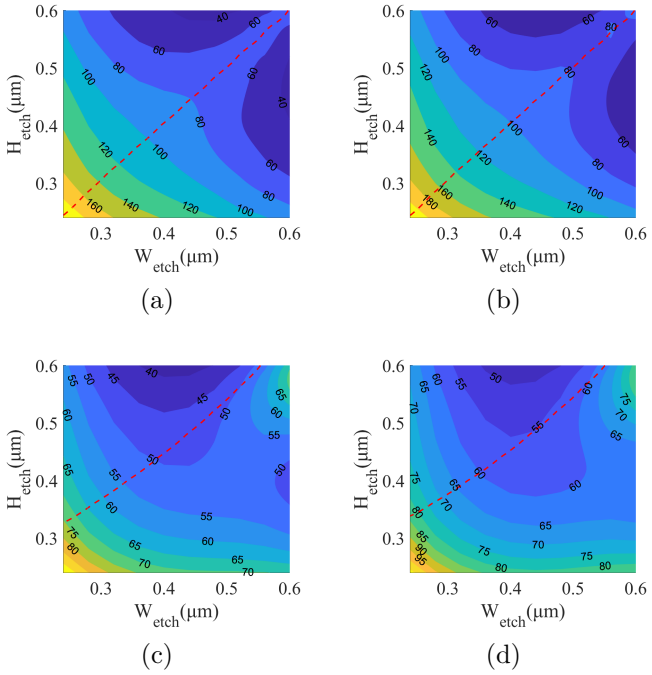

Fig. 3. The calculated beat frequency length Λ with varied H_{etch} ,W_{etch} and duty f. (a)(b) 980 nm ((a)f = 0.3;(a)f = 0.4);(c)(d) 1550 nm ((c)f = 0.3;(d)f = 0.4).

layer, and the Y-axis perpendicular to the waveguide epitaxial layer).The deflection angle θ satisfies the following relationship [40], [41]:

$$\tan(\theta) = \frac{\iint_{Aw} n^2(x,y)e_x^2 dxdy}{\iint_{Aw} n^2(x,y)e_y^2 dxdy} \tag{4}$$

Where $n(x,y)$ is the refractive index distribution in the cross section $e_x(x,y)$ and $e_y(x,y)$ are the transmitted electric field components.

The beat frequency length of the birefringent light is Λ , which is expressed by Equation (5):

$$\Lambda = \frac{\lambda}{n_o - n_e} \tag{5}$$

Where λ is the wavelength ,n_o and n_e are the equivalent refractive indices of the ordinary ray and extraordinary ray, respectively.

In the polarization conversion structure designed in this work, the polarization direction of the incident light is parallel to the fixed coordinate axis of the straight waveguide, and the angle between the incident light and the optical axis in the polarization converter structure is the above optical axis deflection angle θ. After passing half a beat frequency $\frac{\Lambda}{2}$, the polarization direction of the outgoing light and the input light will be deflected by 2θ [42], [43].

By designing the etching depth (H_{etch}), the etching width (W_{etch}) and the duty cycle of the SWG, the polarization rotation of the input linearly polarized light can

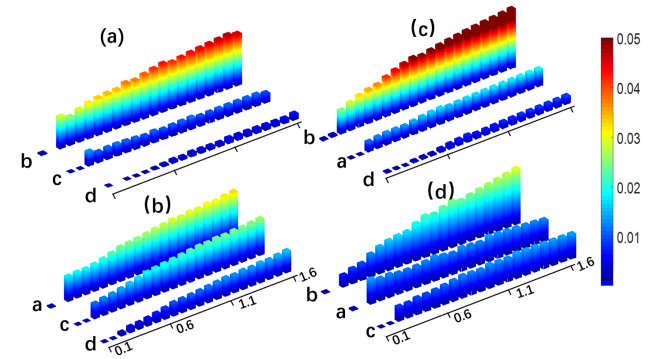

Fig. 4. The calculated effective refractive index mismatch severity of other fundamental modes when one mode is matching in ARW (H_{rib} = 340 nm ,W_{rib} = 600nm and W_{slab} ranges from 0.1 μm to 1.6μm) (a:1550TM_0 ,b:1550TE_0,c:980TM_0 and d:980TE_0)

be realized. The deflection angle and the half-beat length with different structural parameters of the polarization converter are calculated, and the results are shown in Fig. 2 and Fig.3.

Reducing duty cycle of the SWG can lower the required length of PR. However, a high fabrication process is demanded for preparing grating structure with a small duty cycle. Therefore, considering the device length and production preparation, the duty cycle of the SWG structure designed for the PR in this work is set to 0.4. In order to simplify the preparation process, the same height of shadow etching is used for PRs of dual wavelength bands are used. The parameters of the designed subwavelength

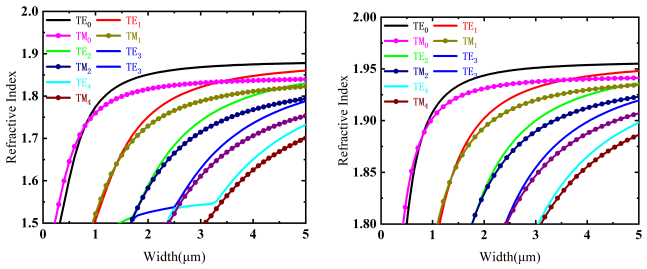

(a) (b)

Fig. 5. The calculated effective refractive index of modes in strip waveguide ((a) 1550nm ,(b)980nm).

grating structure are shown in Table 1.

B. Asymmetric rib polarization beam splitter

The phase matching condition of fundamental mode signals with different wavelengths and polarization could be satisfied at the same time in ADC. A polarization beam splitter (PBS) with low loss and crosstalk is demanded for the (de)MUX. Many excellent PBSs have been reported that can separate signal of dual polarization states well. But few work can support simultaneous beam-splitting of signals with different oscillation directions and wavelengths [44]–[46]. In this work, a PBS based on asymmetric rib waveguide (ARW) is designed, shown in Fig. 1 (c).

Fig.4 shows the phase mismatch severity of other fundamental modes when one mode is matching in ARW where the width of rib is 600nm and slab width ranges from 0.1 μm to 1.6 μm. Polarization and wavelength band beam splitting can be realized with the ARW. Additionally, the ARPBS has a broad operation bandwidth. In order to simplify the preparation difficulty of design, the depth of shallow etching (H_{rib}) is unified to 340 nm , which is same with H_{etch} of PR. The parameters of the designed PBS are shown in Table 2.

C. Asymmetric directional coupler

The cascaded ADCs are used for the transmission and reception of signals from high-ordor modes $(TE(M)_1, TE(M)_2, TE(M)_3)$ of this (de)MUX. The structure of the ADC is shown in Fig. 1 (d). The power conversion between tow waveguides could be solved by coupled-mode theory, shown as follow [47], [48]:

$$\kappa(z) = \frac{sin(\eta z)}{1 + \alpha\left[n_{eff1} - n_{eff2}\right]} \tag{6}$$

Where $\kappa(z)$ is the coupling efficiency of ADCs, α and η are constants determined by couplers, the n_{eff1} and n_{eff2} the refractive indices of modes in each waveguides of ADCs, respectively.

When the fundamental mode signals light from ends of the (de)MUX have phase matching ($n_{eff1} = n_{eff2}$) with the stable mode in the bus waveguide, the uploading and downloading between channel ends and bus could be realized by coupling. Fig .5 illustrates the effective refractive index of each mode at 1550nm and 980nm. The channel information and ADC parameters of the (de)MUX are shown in Table 2.

III. result and analysis

The finite-difference time-domain (FDTD) method is used to study the (de)MUX. Fig. 6 shows the transmission diagram of optical vector in different directions (E_x and E_y) of the SWGPRs of bands centered at 1550 nm and 980 nm. With the TE_0 signal passing through the PR, the E_x component of the input light decreases to zero while

TABLE I
Polarization converter structure parameters

Wavelength Band(nm)	W_pr(μm)	H_pr(μm)	W$_{etch}$(μm)	H$_{etch}$(μm)	P(μm)	f	L$_{PR}$(μm)
1550	0.8	0.8	0.4	0.34	0.2	0.4	56
980	0.8	0.8	0.35	0.34	0.2	0.4	72

TABLE II
Structural parameters of asymmetric directional coupler

Wavelength Band(nm)	Channel	Mode	W$_{wg}$(+0.0m)	W$_{gap}$(μm)	W$_{bus}$(μm)	W$_{rib}$(μm)	W$_{slab}$(μm)	L$_{ADC}$\L$_{PR}$(μm)
1550nm	CH1	TM3	0.8	0.5	4.45	-	-	92
	CH2	TE3	0.8	0.3	3.91	-	-	162
	CH3	TM2	0.8	0.54	3.23	-	-	101
	CH4	TE2	0.8	0.63	2.88	-	-	162
	CH5	TM1	0.8	0.45	2	-	-	62
	CH6	TE1	0.8	0.6	1.84	-	-	102
	CH7	TM0	-	0.5	1	0.8	0.5	106
	CH8	TE0	-	0.62	0.9	0.8	0.3	127
980nm	CH9	TE0	-	0.2	0.98	0.8	0.95	114
	CH10	TM0	-	0.25	0.72	0.6	0.7	60
	CH11	TE1	0.8	0.23	1.725	-	-	110
	CH12	TM1	0.8	0.24	1.835	-	-	108
	CH13	TE2	0.8	0.23	2.65	-	-	141.5
	CH14	TM2	0.8	0.285	2.86	-	-	188
	CH15	TE3	0.8	0.19	3.58	-	-	103
	CH16	TM3	0.8	0.28	3.89	-	-	184

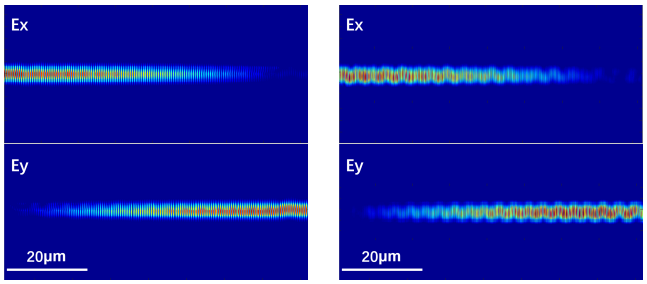

(a) (b)

Fig. 6. The electrical field profiles of E_x and E_y in SWGPRs of two bands ((a) 1550nm (b) 980nm).

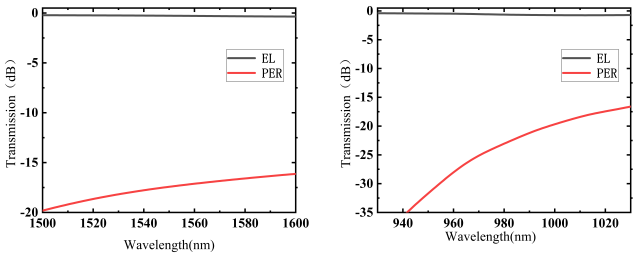

(a) (b)

Fig. 7. The excess loss(EL) and polarization extinction ratio of SWGPRs in this work ((a) 1550nm (b) 980nm).

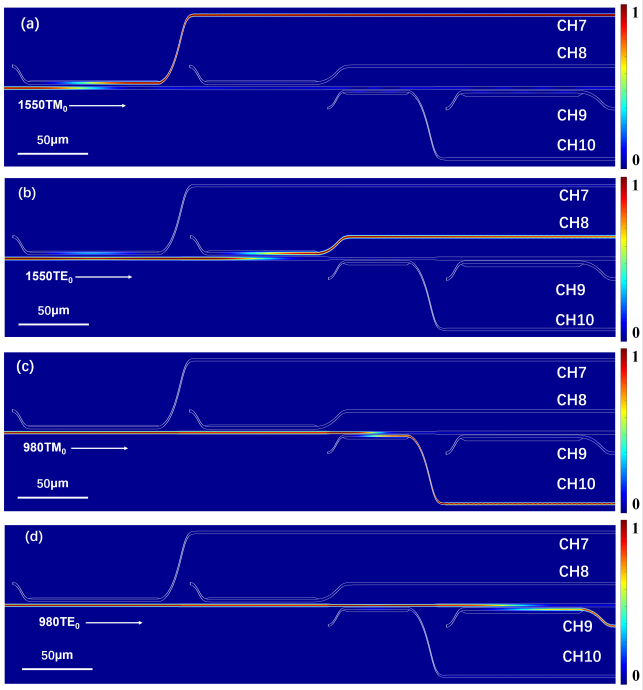

Fig. 8. The numerical simulation profile of the ARPBS with fundamental modes inputs. ((a) 1550 TM_0;(b) 1550 TE_0;(c) 980 TM_0;(d) 980 TE_0).

E_y component gradually increases. This phenomenon demonstrates the conversion between $TE0$ and $TM0$. Fig. 7 illustrates the transmission spectra of the PRs. The subwavelength grating structure exhibits excellent wavelength insensitivity, resulting in high conversion efficiency and low crosstalk ranged a wide spectral. Specifically, the conversion efficiency at 1550 nm is 94% with a crosstalk of -18 dB and the conversion efficiency at 980nm is 86% with a crosstalk of -23 dB. The lower efficiency at 980 nm compared to 1550 nm can be attributed to the higher loss of shorter wavelength in the SWG with the same period.

In order to verify the performance of the PBSs, the fundamental mode signals with different polarization and wavelength are respectively injected into the bus waveguide to observe the transmission effect of each signal ($1550TM_0$(CH7),$1550TE_0$(CH8),$980TM_0$(CH9),and $980TE_0$(CH10)). Fig. 8 shows the light field of the ARPBSs within the (de)MUX. Rare light passes through the waveguide of other channels and few signal light remains in the bus, when only one mode signal is transmitted. Only a small amount of TE_0 light at 1550 nm is coupled into and out of the ADC of CH7 during transmission. The TE_0 and TM_0 modes of various wavelengths transmitted through the bus are fully coupled into the output ends of each channel. Consequently, the ARPBS sequence demonstrates effective polarization isolation and low crosstalk between the 1550 nm and 980 nm bands, enabling the PBS to support the (de)multiplexing of fundamental modes with different polarization states in the dual wavelength band.

The transmission characters of (de)MUX are analyzed, as well. To enhance the demonstration of the performance, we calculate the transmission spectra of the MUX link created by this device. The MUX link is illustrated in Fig.9, and the signal transmission spectra of the link are displayed in Fig.10. The transmission spectral lines of the signal light input from CH1 to CH8, spanning from 1500 nm to 1600 nm, are depicted by solid lines, with the corresponding wavelengths indicated on the lower horizontal axis. Similarly, the transmission spectral lines of the signal light input from CH9 to CH16, ranging from 930 nm to 1030 nm, are represented by dashed lines, and their corresponding wavelengths are shown on the upper horizontal axis. Among them, the TM polarization mode channels have larger loss compared with the TE direction, which is due to the loss introduced by the polarization converter in the incident end and the outgoing end. The transmission spectra of CH9(Fig.9 (i))-CH16(Fig.9 (p)) have more crosstalk from others. That is attributed to the narrow gap of the ADCs and PBSs in the 980 nm band, leading to a reduced phase mismatch between the long-wavelength signal in the bus and the output waveguides [49]. In the 100 nm range of 980 nm and 1550 nm as the center wavelength, the crosstalk is less than -20 dB between the light of the same frequency band and less than -15 dB in almost every channel between different bands. Additionally, the average insertion loss of the (de)MUX link is -1.1 dB.

This article has been accepted for publication in IEEE Photonics Journal. This is the author's version which has not been fully edited and content may change prior to final publication. Citation information: DOI 10.1109/JPHOT.2024.3426933

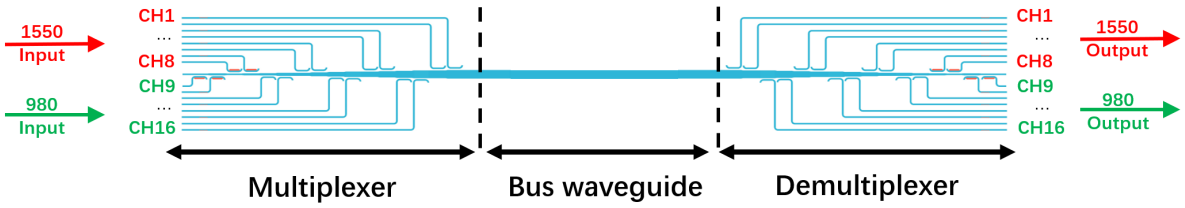

Fig. 9. the schematic of the (de)MUX link formed by the hybrid multiplexers.

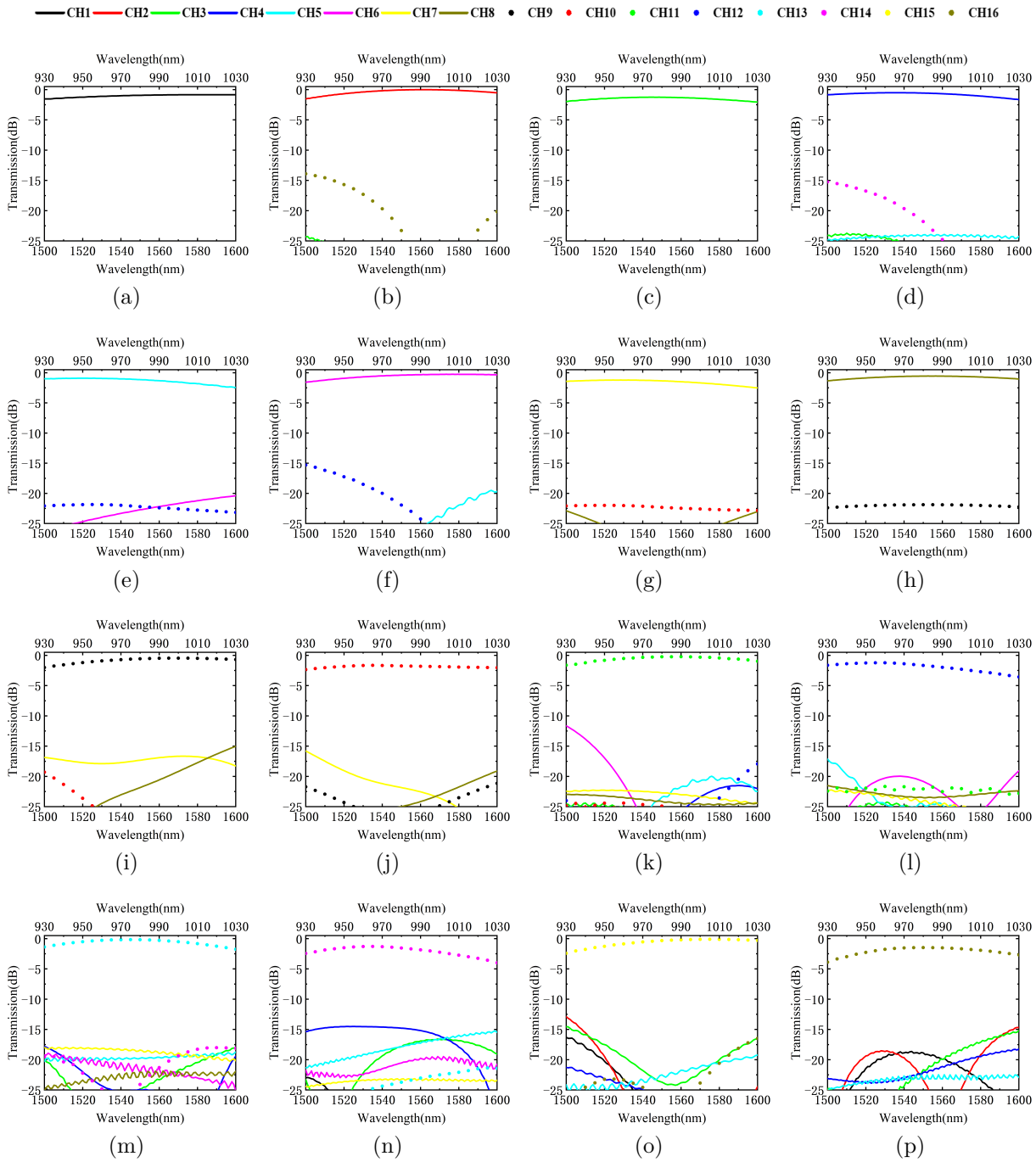

Fig. 10. The transmission spectra of each channels.((a)∼(h)The channels of the band centered at 1550nm, the wavelength coordinates are located on the lower axis of the figure; (i)∼(p)The channels of the band centered at 980nm, the wavelength coordinates are located on the upper axis of the figure)

IV. Conclusion

In this study, a MB hybrid (de)MUX based on 800nm thick Si_3N_4 platform for large-capacity optical transmission system has been developed. The ARW structure serves as the PBS to facilitate polarization beam splitting and decrease crosstalk among different bands. Each component in the multiplexer is wavelength-insensitive, ensuring a vast operational bandwidth. This design offer 16 channels with WDM-PDM-MDM technology,consisting of two frequency bands, dual polarization and four transmission modes (2×2×4). The bandwidth across 670 nm band has been achieved and within the wavelength ranges of 100 nm centered at 980 nm and 1550 nm, the crosstalks of the same frequency band are less than -20 dB , the crosstalks of different frequency band channels are almost always less than -15 dB, and the average insertion loss is -1.1 dB.

With the board bandwidth and multi bands, this (de)MUX could support large number of channels, paving the way for high-capacity optical network. Additionally, this device can support a versatile platform for on-chip few-mode amplifier chip development by integrating both the pump and communication bands. As the core component of multi-band integrated systems, this design also has great potential applications in sensing, optoelectronic computing, and other fields. To the best of our knowledge, this device is the first hybrid (de)MUX chip enabling simultaneous transmission across the 980 nm and 1550 nm bands within a single device.

References

[1] N. Deng, L. Zong, H. Jiang, Y. Duan, and K. Zhang, "Challenges and enabling technologies for multi-band wdm optical networks," Journal of Lightwave Technology, vol. 40, no. 11, pp. 3385–3394, 2022.

[2] A. Ferrari, A. Napoli, J. K. Fischer, N. Costa, A. D'Amico, J. Pedro, W. Forysiak, E. Pincemin, A. Lord, A. Stavdas et al., "Assessment on the achievable throughput of multi-band itu-t g. 652. d fiber transmission systems," Journal of Lightwave Technology, vol. 38, no. 16, pp. 4279–4291, 2020.

[3] A. Mitra, D. Semrau, N. Gahlawat, A. Srivastava, P. Bayvel, and A. Lord, "Effect of channel launch power on fill margin in c+ l band elastic optical networks," Journal of Lightwave Technology, vol. 38, no. 5, pp. 1032–1040, 2020.

[4] H. Shen, M. H. Khan, L. Fan, L. Zhao, Y. Xuan, J. Ouyang, L. T. Varghese, and M. Qi, "Eight-channel reconfigurable microring filters with tunable frequency, extinction ratio and bandwidth," Optics express, vol. 18, no. 17, pp. 18 067–18 076, 2010.

[5] N. Sambo, A. Ferrari, A. Napoli, N. Costa, J. Pedro, B. Sommerkorn-Krombholz, P. Castoldi, and V. Curri, "Provisioning in multi-band optical networks," Journal of Lightwave Technology, vol. 38, no. 9, pp. 2598–2605, 2020.

[6] H. Liu, C. F. Lam, and C. Johnson, "Scaling optical interconnects in datacenter networks opportunities and challenges for wdm," in 2010 18th IEEE Symposium on High Performance Interconnects. IEEE, 2010, pp. 113–116.

[7] D. Dai, "Silicon mode-(de) multiplexer for a hybrid multiplexing system to achieve ultrahigh capacity photonic networks-on-chip with a single-wavelength-carrier light," in 2012 Asia Communications and Photonics Conference (ACP). IEEE, 2012, pp. 1–3.

[8] D. Dai, J. Wang, S. Chen, S. Wang, and S. He, "Monolithically integrated 64-channel silicon hybrid demultiplexer enabling simultaneous wavelength-and mode-division-multiplexing," Laser & Photonics Reviews, vol. 9, no. 3, pp. 339–344, 2015.

[9] D. J. Richardson, J. M. Fini, and L. E. Nelson, "Space-division multiplexing in optical fibres," Nature photonics, vol. 7, no. 5, pp. 354–362, 2013.

[10] D. Dai, J. Wang, and Y. Shi, "Silicon mode (de) multiplexer enabling high capacity photonic networks-on-chip with a single-wavelength-carrier light," Optics letters, vol. 38, no. 9, pp. 1422–1424, 2013.

[11] A. Caut, M. Girardi, V. Torres-Company, A. Larsson, and M. Karlsson, "Channel scalability of silicon nitride (de-) multiplexers for optical interconnects at 1 μm," Journal of Lightwave Technology, 2023.

[12] P. Wolf, P. Moser, G. Larisch, W. Hofmann, and D. Bimberg, "High-speed and temperature-stable, oxide-confined 980-nm vcsels for optical interconnects," IEEE Journal of Selected Topics in Quantum Electronics, vol. 19, no. 4, pp. 1 701 207–1 701 207, 2013.

[13] Z. Chen, L. Wan, S. Gao, K. Zhu, M. Zhang, Y. Li, X. Huang, and Z. Li, "On-chip waveguide amplifiers for multi-band optical communications: a review and challenge," Journal of Lightwave Technology, vol. 40, no. 11, pp. 3364–3373, 2022.

[14] T. Xu, T. Gao, Y. Wang, W. Li, W. Li, C. Du, Z. Yang, Y. Liu, and L. Zhang, "High-gain integrated in-line few-mode amplifier enabling 3840-km long-haul transmission," Photonics Research, vol. 10, no. 12, pp. 2794–2801, 2022.

[15] J. Han, R. Bao, R. Wu, Z. Liu, Z. Wang, C. Sun, Z. Zhang, M. Li, Z. Fang, M. Wang et al., "On-chip wavelength division multiplexing by angled multimode interferometer fabricated on erbium-doped thin film lithium niobate on insulator," arXiv preprint arXiv:2401.05970, 2024.

[16] L.-W. Luo, N. Ophir, C. P. Chen, L. H. Gabrielli, C. B. Poitras, K. Bergmen, and M. Lipson, "Wdm-compatible mode-division multiplexing on a silicon chip," Nature communications, vol. 5, no. 1, pp. 1–7, 2014.

[17] H. Long, W. Wu, Z. Qi, and C. Wang, "Design of an on-chip optical beamforming network based on dense wavelength division multiplexing," in Advanced Optical Manufacturing Technologies and Applications 2022; and 2nd International Forum of Young Scientists on Advanced Optical Manufacturing (AOMTA and YSAOM 2022), vol. 12507. SPIE, 2023, pp. 568–571.

[18] Q. Sun, H. Chen, J. Wang, J. Yang, and H. Jia, "Broadband mode-division (de) multiplexer using nanorod-assisted multimode subwavelength gratings," Optics Communications, vol. 552, p. 130037, 2024.

[19] Q. Huang, J. He, Z. Zheng, and X. Zhou, "Ultra-broadband and low-modal-crosstalk mode multiplexer based on cascaded vertical directional couplers formed by adiabatic-tapered waveguides without mode conversion," Journal of Lightwave Technology, 2023.

[20] W. Jiang, L. Xie, and L. Zhang, "Design and experimental demonstration of a silicon five-mode (de) multiplexer based on multi-phase matching condition," Optics Express, vol. 31, no. 20, pp. 33 343–33 354, 2023.

[21] L. Xu, Y. Wang, D. Mao, J. Zhang, Z. Xing, E. El-Fiky, M. G. Saber, A. Kumar, Y. D'Mello, M. Jacques et al., "Ultra-broadband and compact two-mode multiplexer based on subwavelength-grating-slot-assisted adiabatic coupler for the silicon-on-insulator platform," Journal of Lightwave Technology, vol. 37, no. 23, pp. 5790–5800, 2019.

[22] Y. He, Y. Zhang, X. Jiang, C. Qiu, and Y. Su, "On-chip silicon three-mode (de) multiplexer employing subwavelength grating structure," in 2017 European Conference on Optical Communication (ECOC). IEEE, 2017, pp. 1–3.

[23] R. B. Priti, H. P. Bazargani, Y. Xiong, and O. Liboiron-Ladouceur, "Mode selecting switch using multimode interference for on-chip optical interconnects," Optics Letters, vol. 42, no. 20, pp. 4131–4134, 2017.

[24] J. Wang, S. He, and D. Dai, "On-chip silicon 8-channel hybrid (de) multiplexer enabling simultaneous mode-and polarization-division-multiplexing," Laser & Photonics Reviews, vol. 8, no. 2, pp. L18–L22, 2014.

[25] J.-Y. Su, H.-L. Xu, Z.-Z. Fang, J.-Y. Zhou, and Z.-M. Meng, "Inverse design of a silicon-based ultra-compact four-channel mode splitter with dual polarizations," Optics Communications, p. 130461, 2024.

[26] X. Han, Y. Jiang, A. Frigg, H. Xiao, P. Zhang, T. G. Nguyen, A. Boes, J. Yang, G. Ren, Y. Su et al., "Mode and polarization-division multiplexing based on silicon nitride loaded lithium niobate on insulator platform," Laser & Photonics Reviews, vol. 16, no. 1, p. 2100529, 2022.

[27] X. Fu, J. Niu, Y. Huo, S. Yang, and L. Yang, "Polarization-independent reconfigurable wdm-mdm hybrid multiplexer on silicon photonics platform," IEEE Photonics Technology Letters, vol. 35, no. 8, pp. 438–441, 2023.

[28] S. Ohta, T. Fujisawa, S. Makino, T. Sakamoto, T. Matsui, K. Tsujikawa, K. Nakajima, and K. Saitoh, "Si-based mach-zehnder wavelength/mode multi/demultiplexer for a wdm/mdm transmission system," Optics express, vol. 26, no. 12, pp. 15 211–15 220, 2018.

[29] Y.-D. Yang, Y. Li, Y.-Z. Huang, and A. W. Poon, "Silicon nitride three-mode division multiplexing and wavelength-division multiplexing using asymmetrical directional couplers and microring resonators," Optics express, vol. 22, no. 18, pp. 22 172–22 183, 2014.

[30] Z. Zhou, B. Bai, and L. Liu, "Silicon on-chip pdm and wdm technologies via plasmonics and subwavelength grating," IEEE Journal of Selected Topics in Quantum Electronics, vol. 25, no. 3, pp. 1–13, 2018.

[31] Y. Tan, H. Wu, and D. Dai, "Silicon-based hybrid (de) multiplexer for wavelength-/polarization-division-multiplexing," Journal of Lightwave Technology, vol. 36, no. 11, pp. 2051–2058, 2017.

[32] S. Chen, Y. Shi, S. He, and D. Dai, "Compact monolithically-integrated hybrid (de) multiplexer based on silicon-on-insulator nanowires for pdm-wdm systems," Optics Express, vol. 23, no. 10, pp. 12 840–12 849, 2015.

[33] W. Zhao, Y. Peng, X. Cao, S. Zhao, R. Liu, Y. Wei, D. Liu, X. Yi, S. Han, Y. Wan et al., "96-channel on-chip reconfigurable optical add-drop multiplexer for multidimensional multiplexing systems," Nanophotonics, vol. 11, no. 18, pp. 4299–4313, 2022.

[34] D. J. Moss, R. Morandotti, A. L. Gaeta, and M. Lipson, "New cmos-compatible platforms based on silicon nitride and hydex for nonlinear optics," Nature photonics, vol. 7, no. 8, pp. 597–607, 2013.

[35] P. Munoz, P. W. van Dijk, D. Geuzebroek, M. Geiselmann, C. Dominguez, A. Stassen, J. D. Doménech, M. Zervas, A. Leinse, C. G. Roeloffzen et al., "Foundry developments toward silicon nitride photonics from visible to the mid-infrared," IEEE Journal of Selected Topics in Quantum Electronics, vol. 25, no. 5, pp. 1–13, 2019.

[36] R. Halir, P. J. Bock, P. Cheben, A. Ortega-Moñux, C. Alonso-Ramos, J. H. Schmid, J. Lapointe, D.-X. Xu, J. G. Wangüemert-Pérez, Í. Molina-Fernández et al., "Waveguide sub-wavelength structures: a review of principles and applications," Laser & Photonics Reviews, vol. 9, no. 1, pp. 25–49, 2015.

[37] H. Xu and Y. Shi, "Subwavelength-grating-assisted silicon polarization rotator covering all optical communication bands," Optics Express, vol. 27, no. 4, pp. 5588–5597, 2019.

[38] L. Liu, Q. Deng, and Z. Zhou, "Subwavelength-grating-assisted broadband polarization-independent directional coupler," Optics letters, vol. 41, no. 7, pp. 1648–1651, 2016.

[39] C. Gu and P. Yeh, "Form birefringence dispersion in periodic layered media," Optics letters, vol. 21, no. 7, pp. 504–506, 1996.

[40] L. Gao, F. Hu, X. Wang, L. Tang, and Z. Zhou, "Ultracompact and silicon-on-insulator-compatible polarization splitter based on asymmetric plasmonic–dielectric coupling," Applied Physics B, vol. 113, pp. 199–203, 2013.

[41] V. P. Tzolov and M. Fontaine, "A passive polarization converter free of longitudinally-periodic structure," Optics Communications, vol. 127, no. 1-3, pp. 7–13, 1996.

[42] H. Heidrich, P. Albrecht, M. Hamacher, H.-P. Nolting, H. Schroeter-Janssen, and C. Weinert, "Passive mode converter with a periodically tilted inp/gainasp rib waveguide," IEEE Photonics Technology Letters, vol. 4, no. 1, pp. 34–36, 1992.

[43] Z. Wang and D. Dai, "Ultrasmall si-nanowire-based polarization rotator," JOSA B, vol. 25, no. 5, pp. 747–753, 2008.

[44] Z. Wang, X. Hou, Z. Li, and J. Zhang, "Research on a broadband compact polarization beam splitter," Journal of Russian Laser Research, pp. 1–10, 2024.

[45] Z. Mokeddem, L. Vivien, D. Marris-Morini, E. Cassan, P. Cheben, J. Schmid, D.-X. Xu, Y. Grinberg, M. Milanizadeh, C. Ramos et al., "Experimental demonstration of a sin integrated polarization beam splitter for the 950 nm wavelength band," in Photonic Instrumentation Engineering XI. SPIE, 2024, p. PC1289302.

[46] L. Liu, Q. Deng, and Z. Zhou, "Manipulation of beat length and wavelength dependence of a polarization beam splitter using a subwavelength grating," Optics letters, vol. 41, no. 21, pp. 5126–5129, 2016.

[47] H. Shu, B. Shen, Q. Deng, M. Jin, X. Wang, and Z. Zhou, "A design guideline for mode (de) multiplexer based on integrated tapered asymmetric directional coupler," IEEE Photonics Journal, vol. 11, no. 5, pp. 1–12, 2019.

[48] A. Yariv, "Coupled-mode theory for guided-wave optics," IEEE Journal of Quantum Electronics, vol. 9, no. 9, pp. 919–933, 1973.

[49] B. Ni and J. Xiao, "Ultracompact and broadband silicon-based polarization beam splitter using an asymmetrical directional coupler," IEEE Journal of Quantum Electronics, vol. 53, no. 4, pp. 1–8, 2017.